Investigation of the level structure of $^{91-94}$Zr nuclei using large-scale shell-model calculations*

Bin-Ran Tan (谭彬然)[1] Hao-Yu Jiang (江昊宇)[1] H. K. Wang (王韩奎)[1†] Zhi-Hong Li (李志宏)[2,3‡]

[1]Department of Physics, Zhejiang SCI-TECH University, Hangzhou 310018, China
[2]China Institute of Atomic Energy, P.O. Box 275(10), Beijing 102413, China
[3]School of Nuclear Science and Technology, University of Chinese Academy of Sciences, Beijing 101408, China

Abstract: A suitable Hamiltonian was designed for the Zr isotopes over the $N = 50$ shell by including shell model space between ^{78}Ni and ^{132}Sn. The Hamiltonian is composed by the pairing-plus-multipole force and monopole correction terms. The single-particle energies (SPEs) were initially taken from the low-lying states of hole nuclei ^{131}In and ^{131}Sn (near the $N = 82$ shell closure). These SPEs were then modified by three monopole correction terms to better describe the low-lying states of ^{91}Zr (near the $N = 50$ shell closure). To test this Hamiltonian, the level spectra of $^{91-94}$Zr were investigated in both low-lying and high-spin excitations by large-scale shell-model calculations. Their wave functions were further tested by comparing the electromagnetic transition probabilities with given $B(E2)$ data. The good performance in both spectra and transitions probabilities makes the predicting calculations of the present interaction more dependable to be referred in further experimental researches of Zr isotopes.

Keywords: level structure, shell model, monopole correction, electromagnetic transitions

DOI: 10.1088/1674-1137/ae43c5 **CSTR:** 32044.14.ChinesePhysicsC.50054105

I. INTRODUCTION

The nuclei region around mass number A = 90 lies close to the first abundance peak of the rapid neutron-capture process (r-process) [1−5]. Key nuclei in this region, such as ^{90}Zr, and ^{90}Mo, play a crucial role in nucleosynthesis networks [6−12]. Their nuclear properties, including masses [13, 14], lifetimes [15−17], and neutron-capture cross-sections [18, 19], directly influence the accuracy of r-process simulations, thereby shaping our understanding of the origin of heavy elements in the universe, particularly in astrophysical events such as neutron-star mergers [20−22].

Zirconium isotopes are of particular importance across multiple disciplines, including nuclear physics, astrophysics, nuclear energy, and geochemistry. Their unique nuclear behavior and chemical stability make them a focal point for both fundamental and applied research. In nuclear energy applications, natural zirconium, composed predominantly of ^{90}Zr, ^{91}Zr, ^{93}Zr, ^{94}Zr, exhibits an exceptionally low thermal-neutron capture cross-section [18, 23−25]. This property renders zirconium alloys the material of choice for fuel-rod cladding and structural components in light-water reactors [26]. Furthermore, ^{95}Zr, a medium-lived fission product (half-life about 64 days), serves as an important monitor of fuel burn-up and fission yield in reactor operations and nuclear tests [27]. Several long-lived radioactive zirconium isotopes also appear in nuclear waste streams, and research on their nuclear properties supports the assessment of waste inventories and the development of potential transmutation strategies [28].

From a nuclear-structure perspective, zirconium isotopes span a critical region of the nuclear chart. Isotope ^{90}Zr, with a neutron number $N = 50$, corresponds to a traditional neutron shell closure. Systematic studies from neutron-deficient species (*e.g.*, ^{80}Zr) to neutron-rich ones (*e.g.*, ^{110}Zr) reveal the evolution of nuclear shell structure [30, 31], the onset of collective deformation [32, 33], and the occurrence of shape coexistence [34−36]. While traditional shell models predict $N = 50$ as a magic number associated with spherical closed shells, experimental evidence indicates significant deformation in many nuclides near this region, reflecting the weakening of magic effects and the evolution of shell structure [37−39].

In this study, a suitable shell model interaction was designed for describing the level structure of Zr isotopes (A >90) in both low-lying and high-spin excitations. This

Received 1 January 2026; Accepted 9 February 2026; Accepted manuscript online 10 February 2026

* Research at ZSTU was supported by the National Natural Science Foundation of China (12475124, U2267205), and ZSTU intramural grant(22062267-Y). Research at China Institute of Atomic Energy was supported by the National Natural Science Foundation of China (12475151)

† E-mail: whk@zstu.edu.cn

‡ E-mail: zhli@ciae.ac.cn

interaction includes the pairing-plus-multipole force and the monopole corrections in the shell model space with four proton and five neutron orbits between ^{78}Ni and ^{132}Sn. Section II describes the interaction model framework. Section III shows its performance in the level spectra of nuclei $^{91-94}$Zr, as well as electromagnetic transitions probabilities. Section IV presents the conclusions. The shell-model code NUSHELL@MSU was used for the calculations [40].

II. HAMILTONIAN

The shell model space includes five neutron levels below the neutron magic number $N = 82$ ($0g_{7/2}$, $1d_{5/2}$, $2s_{1/2}$, $0h_{11/2}$, $1d_{3/2}$) and four proton levels below the proton magic number $N = 50$ ($0f_{5/2}$, $1p_{3/2}$, $1p_{1/2}$, $0g_{9/2}$), with the frozen core ^{78}Ni. The single particle states of these orbits are referred from Ref. [41], which selected from the low-lying levels of single hole nuclei ^{131}In and ^{131}Sn under ^{132}Sn. The Hamiltonian of this model space is expressed in the proton-neutron (pn) representation as follows:

$$\begin{aligned} H &= H_{SP} + H_{P_0} + H_{P_2} + H_{QQ} + H_{OO} + H_{HH} + H_{mc} \\ &= \sum_{\alpha,i} \epsilon_a^i c_{\alpha,i}^\dagger c_{\alpha,i} - \frac{1}{2}\sum_{I=0,2}\sum_{ii'} g_I, ii' \sum_M P_{IM,ii'}^\dagger P_{IM,ii'} \\ &\quad - \frac{1}{2}\sum_{ii'} \frac{\chi_{2,ii'}}{b^4} \sum_M :Q_{2M,ii'}^\dagger Q_{2M,ii'}: \\ &\quad - \frac{1}{2}\sum_{ii'} \frac{\chi_{3,ii'}}{b^6} \sum_M :O_{3M,ii'}^\dagger O_{3M,ii'}: \\ &\quad - \frac{1}{2}\sum_{ii'} \frac{\chi_{4,ii'}}{b^8} \sum_M :H_{4M,ii'}^\dagger H_{4M,ii'}: \\ &\quad + \sum_{a\le c,ii'} k_{mc}(ia,i'c) \sum_{IM} A_{IM}^\dagger(ia,i'c) A_{IM}(ia,i'c). \end{aligned} \tag{1}$$

Eq. (1) includes the single-particle Hamiltonian ($H_{\rm sp}$), the $J = 0$ and $J = 2$ pairings ($P_0^\dagger P_0$ and $P_2^\dagger P_2$), the quadrupole-quadrupole ($Q^\dagger Q$), the octupole-octupole ($O^\dagger O$), the hexadecapole-hexadecapole ($H^\dagger H$) terms, and the monopole corrections ($H_{\rm mc}$). In the pn representation, $P_{JM,ii'}^\dagger$ and $A_{JM}^\dagger(ia,i'b)$ are the pair operators, and $Q_{2M,ii'}^\dagger$, $O_{3M,ii'}^\dagger$, and $H_{4M,ii'}^\dagger$ are the quadrupole, octupole, and hexadecapole operators, respectively, where i and i' are indices for proton or neutron. The constants $g_{J,ii'}$, $\chi_{2,ii'}$, $\chi_{3,ii'}$, $\chi_{4,ii'}$, and $k_{\rm mc}(ia,i'b)$ are the corresponding force strengths, and b is the harmonic-oscillator range parameter. The force strengths of the Hamiltonian are listed in Table 1. In Ref. [42], the monopole and multipole effects were examined carefully by using the generator-coordinate method. In this study, three monopole correction terms were incorporated to apply the interaction to Zr isotopes near $A = 90$:

Table 1. Two-body force strengths (in MeV).

ii'	$g_{0,ii'}$	$g_{2,ii'}$	$\chi_{2,ii'}$	$\chi_{3,ii'}$	$\chi_{4,ii'}$
pp	39	350	600	550	0.0014
nn	18	320	400	70	0.0008
np	0	0	200	0	0.0009

$$\begin{aligned} Mc1 &\equiv k_{\rm mc}(\nu g_{7/2}, \nu g_{7/2}) = -0.9 \text{ MeV}, \\ Mc2 &\equiv k_{\rm mc}(\pi g_{9/2}, \nu g_{7/2}) = -0.2 \text{ MeV}, \\ Mc3 &\equiv k_{\rm mc}(\pi g_{9/2}, \nu s_{1/2}) = -0.07 \text{ MeV}. \end{aligned} \tag{2}$$

As shown in Fig. 1, their effects are demonstrated by adding the three monopole terms one by one. For easy comparison of calculations with the corresponding data, the difference factor is defined as the ratio of the theoretical value to the corresponding datum. After only considering Mc1, bottom level $7/2^+$ clearly shifts up, while level $5/2^+$ goes down as the ground state in both ^{91}Zr and ^{93}Zr. Terms Mc2 and Mc3 clearly improve level $1/2^+$ of ^{91}Zr (^{93}Zr) with a difference factor 1.06 (0.98) in comparison with columns "+Mc1" and "+Mc3". In ^{92}Zr (^{94}Zr), levels 2^+ and 4^+ are affected slightly with monopole corrections, while level 6^+ clearly shifts up with a difference factor 0.99 (0.92) in comparison with columns "+Mc0" and "+Mc3". The second 0^+ and 2^+ of ^{92,94}Zr are notably improved in terms of both excited energies and orders. The cross-subshell was reported in Ref. [43]. As shown in Fig. 1, the proportion of cross-subshell Z = 40 is listed as WI/WO, which means the ratio with and without orbit $\pi g_{9/2}$ up Z = 40. In low-lying levels, the cross-subshell share clearly decreases as a result of including monopole corrections.

III. RESULTS AND DISCUSSION

A. ^{91}Zr

As a stable single-neutron nucleus, ^{91}Zr has been extensively researched for decades. Arroe and Mack first studied the optical hyperfine structure of Zr, obtaining a nuclear spin of 5/2 for ^{91}Zr [44]. Ground state $5/2^+$ is formed by coupling proton holes in the $p_{1/2}$ and $g_{9/2}$ orbits with a neutron particle in the $d_{5/2}$ orbital. Low-lying excited states $1/2^+$ and $7/2^+$ arise from coupling the same proton holes with a neutron particle in the $s_{1/2}$ and $d_{5/2}$ orbits, respectively. As shown in Fig. 2, ground state $5/2^+$ has 49.17% of configuration $\pi p_{1/2}^{-2} g_{9/2}^{-8} \nu d_{5/2}^1$ and 44.35% of configuration $\pi g_{9/2}^{-10} \nu d_{5/2}^1$ The main configurations of the excited states $1/2^+$ and $7/2^+$ are 50.63% $\pi p_{1/2}^{-2} g_{9/2}^{-8} \nu s_{1/2}^1$ and 77.54% $\pi p_{1/2}^{-2} g_{9/2}^{-8} \nu d_{5/2}^1$, with difference factors of 1.06 and 1.007, respectively.

High-spin levels in ^{91}Zr have been studied by using

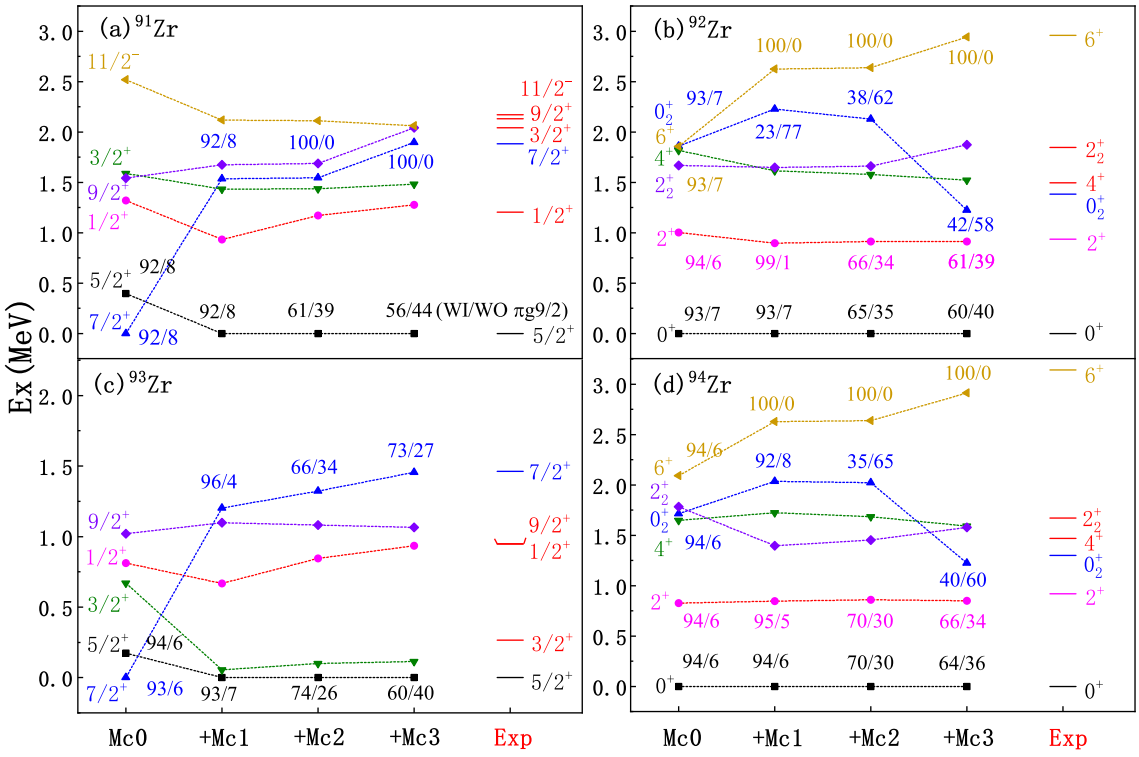

Fig. 1. (color online) Monopole effects in the low-lying levels of $^{91-94}$Zr, data from Ref. [29]. Label WI/WO is the ratio with and without cross-subshell $\pi g_{9/2}$.

the reaction ^{88}Sr(^{6}Li,p2n)^{91}Zr, and the state $|(g_{9/2}p_{1/2}d_{5/2}),15/2^-\rangle$ is located at 2288 keV according to Ref. [45]. In Ref. [46], a $21/2^+$ state at 3167 keV was discovered using the reaction ^{88}Sr(^{6}Li, $p2n$)^{91}Zr. For the two data, calculational levels $15/2^-$ and $21/2^+$ at 1951 keV and 2870 keV have difference factors of 0.85 and 0.9, respectively. The main configuration of the $15/2^-$ level is 96.85% of $\pi p^{-1}_{1/2}g^{-9}_{9/2}\nu d^{1}_{5/2}$. The main configuration of the $21/2^+$ level is 88.01% of $\pi p^{-2}_{1/2}g^{-8}_{9/2}\nu d^{1}_{5/2}$.

The level scheme of ^{91}Zr was extended with the newly $15/2^+$ and $19/2^+$ states at 3.41 and 3.78 MeV in Ref. [48]. In calculations, the $15/2^+$ state at 3.01 MeV has a main configuration of $\pi p^{-2}_{1/2}g^{-8}_{9/2}\nu d^{1}_{5/2}$ with a difference factor of 0.88. The first $19/2^+$ level is located at 3.047 MeV, whereas the second $19/2^+_2$ level is located at 3.953 MeV. The $19/2^+_2$ state has a main configuration of $\pi p^{-1}_{1/2}g^{-9}_{9/2}\nu h^{1}_{11/2}$, with a difference factor of 0.96. The present calculations extend the excited energy to $E_x \approx 10$ MeV. In calculations, the first $29/2^-$ level is located at 7.256 MeV, whereas the second $29/2^-_2$ level is located at 7.393 MeV. The main configuration of $29/2^-_2$ is 96.61% of $\pi p^{-1}_{3/2}p^{-1}_{1/2}g^{-8}_{9/2}\nu h^{1}_{11/2}$, with a difference factor of 1.034 in comparison with datum (29/2) at 7.663 MeV. The configurations of $33/2^+$ and $35/2^+$ are 91.93% and 91.15% $\pi p^{-1}_{3/2}p^{-2}_{1/2}g^{-7}_{9/2}\nu h^{1}_{11/2}$, respectively. Their difference factors are 0.96 and 0.98 in comparison with data (33/2) and (35/2) at 9.129 and 9.462 MeV, respectively. The ratio with and without cross-subshell Z=40 is added as WI/WO in Fig. 2. These quantitative proportions indicate that cross-subshell excitations dominate the low-excitation energy spectra, while the high-energy, high-spin portions of the spectra almost entirely originate from proton excitations across Z=40.

B. ^{92}Zr

In Ref. [50], the properties of the 2^+ states of ^{92}Zr were investigated using non-elastic electron scattering experiments under low momentum transfer conditions. It was confirmed that the transitions to the 2^+_1 and 2^+_2 states primarily follow a monopole substructure mode (Fig. 3). The first excited state 2^+ at 911 keV has 41.68% of configuration $\pi p^{-2}_{1/2}g^{-8}_{9/2}\nu d^{2}_{5/2}$, with a difference factor of 0.97. The second 2^+_2 state at 1.874 MeV has 49.28% of configuration $\pi p^{-2}_{1/2}g^{-8}_{9/2}\nu d^{2}_{5/2}$, with a difference factor of 1.01.In Ref. [51], this state was confirmed at 1.847 MeV by the $(n,n'\gamma)$ reaction.

Ground state 0^+ has two primary configurations: 43.59% of $\pi p^{-2}_{1/2}g^{-8}_{9/2}\nu d^{2}_{5/2}$ and 33.79% of $\pi g^{-10}_{9/2}\nu d^{2}_{5/2}$. The 0^+_2 level at 1224 keV has 48.79% of primary configuration $\pi g^{-10}_{9/2}\nu d^{2}_{5/2}$, with a difference factor of 0.88. The first 4^+ level at 1.520 MeV agrees with datum 1.495 MeV, with a difference factor of 1.01. It has 49.09% of configuration $\pi p^{-2}_{1/2}g^{-8}_{9/2}\nu d^{2}_{5/2}$. The 6^+ and 8^+ states share the same dominant configuration $\pi p^{-2}_{1/2}g^{-8}_{9/2}\nu d^{2}_{5/2}$, 71.01% and 71.3% percentage, respectively. Negative parity level 5^- at 2.014 MeV has a dominant configuration of

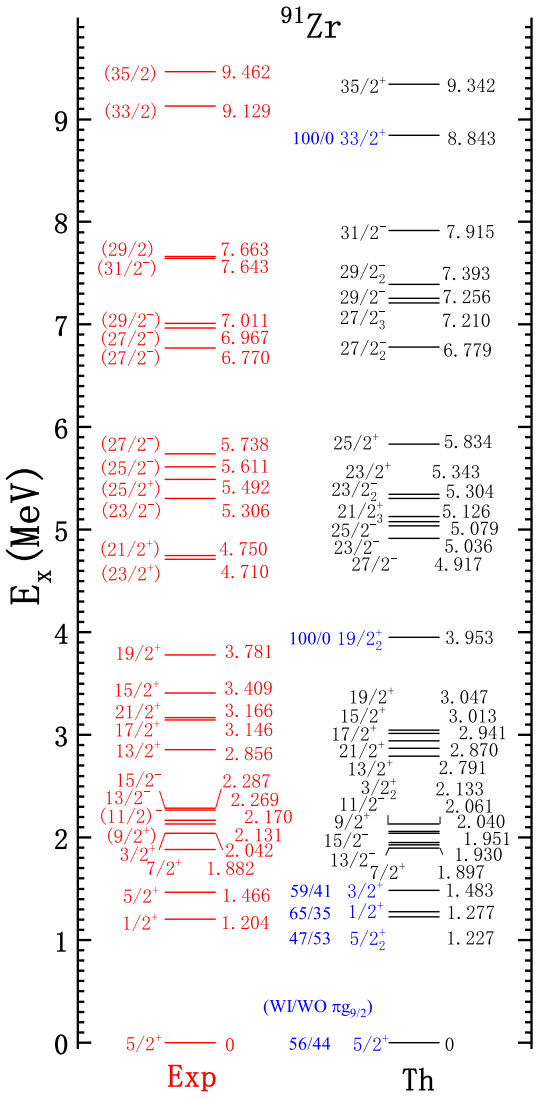

Fig. 2. (color online) Level spectra of ^{91}Zr, data from Refs. [44–48]. Label WI/WO is the ratio with and without cross-subshell $\pi g_{9/2}$.

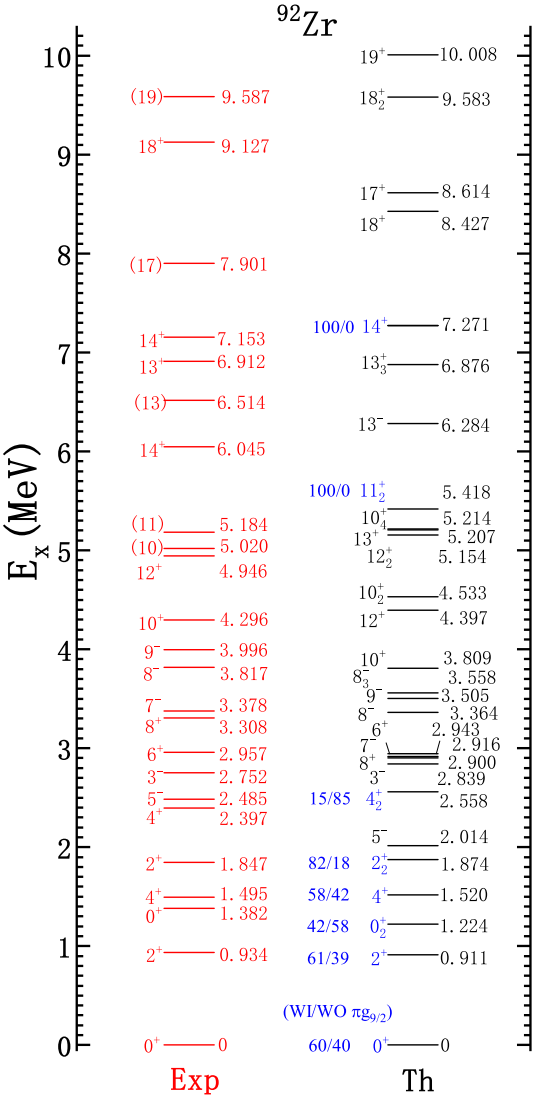

Fig. 3. (color online) Level spectra of ^{92}Zr, data from Refs. [49–55]. Label WI/WO is the ratio with and without cross-subshell $\pi g_{9/2}$.

$\pi p^{-1}_{1/2} g^{-9}_{9/2} \nu d^{2}_{5/2}$, 80.36%. This level was first proposed with (p, p') angular distribution measurements by Dickens et al. in Ref. [52]. Brown *et al.* [53], based on negative coefficient measurements of the transition from 2485 keV to the 4^+ state at 1495 keV, suggested this level as J=3 or 5.

Regarding high-spin states, Brown *et al.* conducted a study on the high spin states of ^{92}Zr through the ^{88}Sr(^{7}Li, $p2n$)^{92}Zr reaction, extending the spectra to 12^+ at 4947 keV [53]. In calculations, the first 12^+ level was located at 4.397 MeV, whereas the second 12^+ was located at 5.154 MeV. The 12^+_2 level has 84.36% of configuration $\pi p^{-2}_{1/2} g^{-8}_{9/2} \nu d^{2}_{5/2}$, with a difference factor of 1.04. Fotiades *et al.* [54] investigated the level structure of ^{92}Zr using the ^{24}Mg + ^{173}Yb reaction. Their research extended the level scheme up to the (18^+) state at $E_x \approx 9127$ keV. The first 18^+ level is located at 8.427 MeV, whereas the second 18^+ is located at 9.583 MeV. The 18^+_2 state has a difference factor of 1.04 in comparison with this datum. It has a dominant configuration of $\pi p^{-1}_{3/2} p^{-2}_{1/2} g^{-7}_{9/2} \nu d^{1}_{5/2} h^{1}_{11/2}$, 90.21% percentage. In 2025, experimental research extended the excited energy of ^{92}Zr to $E_x \approx 10$ MeV with state (19) at 9.587 MeV[55]. The main configuration of level 19^+ is 90.82% of $\pi p^{-1}_{3/2} p^{-2}_{1/2} g^{-7}_{9/2} \nu d^{1}_{5/2} h^{1}_{11/2}$, with a difference factor of 1.04 in comparison with datum (19) at 9.587 MeV.

C. ^{93}Zr

The ground state of ^{93}Zr was confirmed in Ref. [56]. Cohen and Chubinsky [57] performed nuclear reactions, namely pick-up ^{94}Zr(d,t)^{93}Zr and stripping ^{92}Zr(d,p)^{93}Zr, and proposed the $(d_{5/2})^n$ configuration dominating the low-lying level structure of ^{93}Zr. In calculations, the level

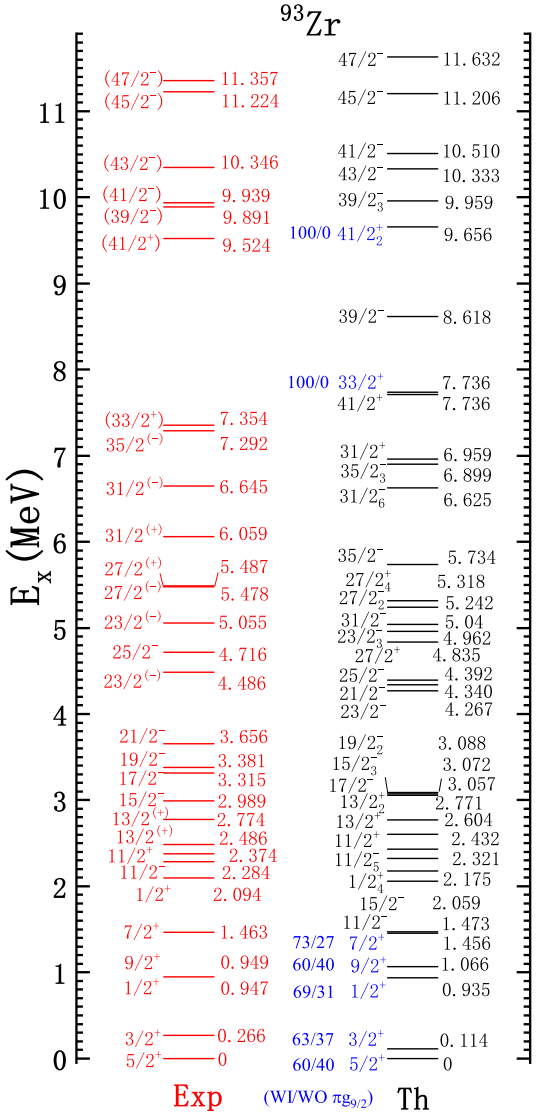

Fig. 4. (color online) Level spectra of ^{93}Zr, data from [54, 56, 60–62]. Label WI/WO is the ratio of with and without cross-subshell $\pi g_{9/2}$.

$5/2^+$ has 43.84% of configuration $\pi p^{-2}_{1/2}g^{-8}_{9/2}\nu d^3_{5/2}$ and 33.62% of configuration $\pi g^{-10}_{9/2}\nu d^3_{5/2}$. In Ref. [58], a state $9/2^+$ was predicted at 1100 keV with configuration $(d_{5/2})^3$. To confirm this prediction, Arad *et al.* measured γ rays from the β decay of the fission product ^{93}Y using a Ge(Li) spectrometer, and tentatively established a level $9/2^+$ at 1167.7 keV [59]. The latest study [60] investigated the excited states of ^{93}Zr via the heavy-ion fusion-evaporation reaction, and identified the $9/2^+$ level at 949 keV. In the present study, level $9/2^+$ at 1.066 MeV has 47.04% of configuration $\pi p^{-2}_{1/2}g^{-8}_{9/2}\nu d^3_{5/2}$ and 36.93% of configuration $\pi g^{-10}_{9/2}\nu d^3_{5/2}$.

Besides low-lying levels, Ref. [54] extended the spectra of ^{93}Zr to approximately 4.5 MeV using the coincidence of γ transitions and their relative intensities. The spectrum of ^{93}Zr was extended to approximately 7 MeV via reaction ^{28}Si + ^{176}Yb and the level at 4716.8 keV, which was assigned a spin-parity of $25/2^+$ for the first time [62]. However, in the latest study, the energy level at 4716 keV was assigned $25/2^-$, and the parity was determined to be negative. In calculations, level $25/2^-$ at 4.392 MeV has 68.67% of configuration $\pi p^{-2}_{1/2}g^{-8}_{9/2}\nu d^2_{5/2}h^1_{11/2}$, with a difference factor of 0.93. In another study [60], the energy spectrum of ^{93}Zr was extended to $E \approx 12.5$ MeV with the spin-parity to $I^\pi = (47/2^-)$. In calculations, level $47/2^-$ at 11.632 MeV has 85.05% of configuration $\pi p^{-1}_{3/2}p^{-2}_{1/2}g^{-7}_{9/2}\nu d^1_{5/2}h^2_{11/2}$, with a difference factor of 1.02. Level $45/2^-$ at 11.206 MeV has 89.96% of configuration $\pi p^{-1}_{3/2}p^{-2}_{1/2}g^{-7}_{9/2}\nu d^1_{5/2}h^2_{11/2}$, and a difference factor of 0.99.

D. ^{94}Zr

The low-spin states of ^{94}Zr were investigated through the β-decay of ^{94}Y in Ref. [66, 67]. The 2^+_2 state at 1671.4 keV was determined via the $(n,n'\gamma)$ reaction [64]. Peters *et al.* [65] measured the energy of 1671 keV again using the Doppler-shift attenuation method (DSAM) and the $(n,n'\gamma)$ reaction, which also reported the second 2^+ state at 1671 keV. As shown in Fig. 5, ground state 0^+ has two primary configurations: $\pi p^{-2}_{1/2}g^{-8}_{9/2}\nu d^4_{5/2}$ (35.51%) and $\pi g^{-10}_{9/2}\nu d^4_{5/2}$ (24.67%). The level 2^+ at 0.849 MeV has 34.58% of configuration $\pi p^{-2}_{1/2}g^{-8}_{9/2}\nu d^4_{5/2}$, with a difference factor of 0.92. The 2^+_2 state at 1579 keV has a difference factor of 0.94, having mixed configurations: 16.21% of $\pi p^{-2}_{1/2}g^{-8}_{9/2}\nu d^3_{5/2}s^1_{1/2}$, 13.02% of $\pi p^{-2}_{1/2}g^{-8}_{9/2}\nu d^4_{5/2}$, and 8.97% of $\pi p^{-2}_{1/2}g^{-8}_{9/2}\nu d^3_{5/2}d^1_{3/2}$. Level 4^+ at 1.592 MeV has 43.86% of configuration $\pi p^{-2}_{1/2}g^{-8}_{9/2}\nu d^4_{5/2}$, with a difference factor of 1.08. Level 4^+_2 at 2.251 Mev has 22.42% of $\pi p^{-2}_{1/2}g^{-8}_{9/2}\nu d^3_{5/2}d^1_{3/2}$ configuration, with a difference factor of 0.96.

Concerning high-spin states, Ref. [54] observed some data from 4812 to 7791 keV via the decay of the compound nucleus ^{197}Pb produced by a ^{24}Mg beam at 134.5 MeV. Based on this study, leveraging the detection of the prompt γ-rays on the EUROGAM II and EUROBALL arrays, Pantelica *et al.* [62] assigned spins and parities of states (12^+) at 4813.8 keV, (11^+) at 5492.9 keV, (12^+_2) at 5806.9 keV, and (13^+) at 6009.51 keV, as well as spin-assigned states (14), (15), and (16), listed at the top of Fig. 5. In calculations, the first 12^+ level at 4.549 MeV has a difference factor of 0.942 in comparison with datum 4.813 MeV. Note that 12^+_3 at 4.829 MeV reproduces well datum 4.813 MeV with a difference factor of 1.003, which has 68.78% of $\pi p^{-1}_{1/2}g^{-9}_{9/2}\nu d^3_{5/2}h^1_{11/2}$ configuration. For the datum (14) at 6.374 MeV, the first 14^+ level at 5.787 MeV has 69.09% of $\pi p^{-1}_{1/2}g^{-9}_{9/2}\nu d^3_{5/2}h^1_{11/2}$ configuration. Level 14^+_3 at 6.131MeV has 45.84% of $\pi g^{-10}_{9/2}\nu d^2_{5/2}h^2_{11/2}$ configuration, with a difference factor of 0.96. The first 15^+ level at 5.849 MeV has 69.93% of $np^{-1}_{1/2}g^{-9}_{9/2}\nu d^3_{5/2}h^1_{11/2}$ configuration Level 15^+_2 at 7.070 MeV has a difference factor 1.001 in comparison with datum (15) at 7.058 MeV,

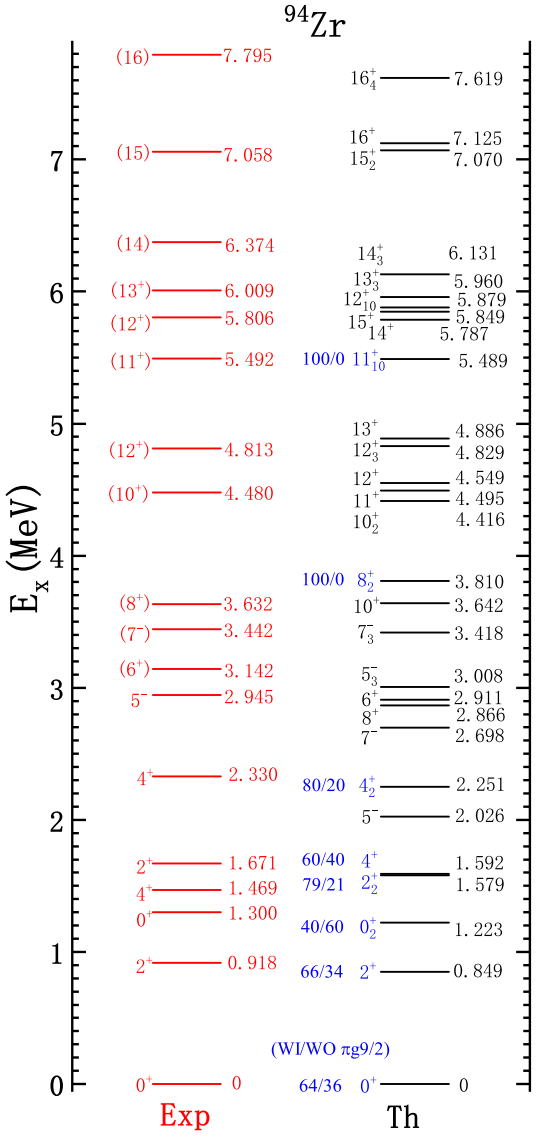

Fig. 5. (color online) Level spectra of ^{94}Zr, data from Refs. [54, 62–65]. Label WI/WO is the ratio with and without cross-subshell $\pi g_{9/2}$

which has 85.84% of $\pi p_{1/2}^{-1} g_{9/2}^{-9} \nu d_{5/2}^2 h_{11/2}^1 d_{3/2}^1$ configuration. The first 16^+ level at 7.125 MeV has 56.71% $\pi p_{1/2}^{-2} g_{9/2}^{-8} \nu d_{5/2}^2 h_{11/2}^2$ configuration. Level 16_4^+ at 7.619 MeV reproduces well datum 7.795 MeV with a difference factor of 0.97, which has 65.32% of $\pi g_{9/2}^{-10} \nu d_{5/2}^2 h_{11/2}^2$ configuration.

E. Electromagnetic transitions

Electric quadrupole transitions reflect the degree of collective nuclear deformation, which is described by the transition probability $B(E2)$. The transition probabilities are stringent tests for the wave function of energy levels. The isomerism was discussed using lifetimes in the southeastern vicinity of ^{208}Pb[68].

In Table 2, we list the $B(E2)$ values with lifetimes.

The value 3.68 W.u. of $B(E2;1/2^+ \to 5/2^+)$ has a difference factor of 0.24 in comparison with datum 15 W.u. of ^{91}Zr. The value 2.03 W.u. from the second $1/2^+$ level has a difference factor of 0.78 with datum 1.6 W.u. The $E2$ values from $7/2^+$ and $9/2^+$ to the ground state reproduce well data 7.7 and 4.2 W.u. In ^{92}Zr, the value 2.1 W.u. of $B(E2;2^+ \to 0^+)$ has a difference factor of 0.32 in comparison with datum 6.4 W.u. The value 3.79 W.u. from the second 2^+ level has a remarkable difference factor of 1.02 with datum 3.7 W.u.

In ^{93}Zr, the value 4.45 W.u. of $B(E2;3/2^+ \to 5/2^+)$ has a difference factor of 0.63 in comparison with datum 7(6) W.u. The $B(E2)$ value from second $3/2^+$ to ground state $5/2^+$ is 0.73 W.u. For other $B(E2)$ transitions, no more experimentally measured values are available, and we theoretically calculated those from several low-lying excited states to the ground state. For example, the value of $B(E2;1/2^+ \to 5/2^+)$ is 1.61 W.u., and the second $1/2^+$ state to ground state $5/2^+$ is 3.71 W.u. The value of $B(E2;9/2^+ \to 5/2^+)$ is 1.73 W.u. and the second $1/2^+$ state to ground state $5/2^+$ is 4.39 W.u.

In ^{94}Zr, $B(E2;2_1^+ \to 0_1^+)$ was calculated to be 4.9 (11) W.u. via the (n, n') reaction according to the Doppler Shift Attenuation Method (DSAM) [69]. As shown in Table 2, the corresponding value is 2.57 W.u. with a difference factor of 0.52. The $B(E2)$ value from second 2^+ to ground state 0^+ is 3.27 W.u., with a difference factor of 0.83 in comparison with datum 3.9 W.u. The value 0.55 W.u. from 4^+ to 2^+ properly reproduces the corresponding datum 0.88(23). Several experimental $B(E2)$ transition probabilities have been observed to significantly exceed calculations. Notable examples include $B(E2;3/2^+ \to 5/2^+) = 59(6)$ W.u. in ^{91}Zr, $B(E2;10_1^+ \to 8_1^+) = 31^{+5}_{-4}$ W.u in ^{92}Zr, and $B(E2;4_2^+ \to 2_2^+) = 34^{+10}_{-7}$ W.u. in ^{94}Zr. As reported in Ref. [69], the $B(E2)$ values in ^{94}Zr provide direct evidence for a consistent picture of shape coexistence. Furthermore, Ref. [70] reports a large $B(E2)$ value in ^{92}Zr and proposes, within a phenomenological deformed rotor model, that the observed nuclear collectivity may originate from a coexisting deformed structure. The consistently enhanced $B(E2)$ values across these Zr isotopes indicate the nuclear collectivity in this region, while a truncated model space severely limits the ability of the shell model to describe nuclear collective effects.

IV. SUMMARY

In this study, a suitable interaction was designed for investigating the level structure of Zr isotopes over $N = 50$ shell. The interaction is composed by the pairing-plus-multipole force and monopole correction terms. Three monopole correction terms were added to modify the single particle states of ^{132}Sn to adapt to the low-lying states of ^{91}Zr close to the $N = 50$ shell. The present interaction properly describes the level structure of $^{91-94}$Zr in

Table 2. Electric quadrupole transitions [29, 64, 69–71].

^{Z}X	Transition(W.u.)	τL	Exp.	τ/ps	Th.	τ/ps
^{91}Zr	$1/2^+ \to 5/2^+$	$E2$	15(4)	0.89	3.68	1.86
	$1/2^+_2 \to 5/2^+$	$E2$	1.6^{+5}_{-8}	0.19	2.03	0.26
	$7/2^+ \to 5/2^+$	$E2$	7.7(13)	0.109	4.93	0.13
	$7/2^+_2 \to 5/2^+$	$E2$	1.15^{+21}_{-32}	$0.48^{+13}_{-8.7}$	0.09	0.81
	$3/2^+ \to 5/2^+$	$E2$	59(6)	0.016	0.68	0.005
	$3/2^+_2 \to 5/2^+$	$E2$			3.32	
	$3/2^+_3 \to 5/2^+$	$E2$		0.024	0.01	0.09
	$9/2^+ \to 5/2^+$	$E2$	4.2(6)	0.163	4.28	0.15
	$(13/2)^+ \to (9/2^+)$	$E2$	> 0.0079		7.73	
	$(13/2)^+_2 \to (9/2^+)$	$E2$			0.87	
	$(17/2)^+ \to (13/2^+)$	$E2$	> 0.19		5.48	
	$(17/2)^+_2 \to (13/2^+)$	$E2$			0.37	
^{92}Zr	$2^+ \to 0^+$	$E2$	$6.4^{+0.6}_{-0.5}$[71]	7.21(58)	2.1	1.727
	$2^+_2 \to 0^+$	$E2$	3.4(4)[71]	0.138(14)	3.79	0.25
	$2^+_3 \to 0^+$	$E2$	< 0.005[71]	> 1.1	0.19	2.27
	$2^+_4 \to 0^+$	$E2$	0.048(7)	0.092(10)	0.36	1.01
	$2^+_5 \to 0^+$	$E2$			0.001	
	$4^+ \to 2^+$	$E2$	4.05(11)[71]	0.147(4)	1.26	2.15
	$4^+_2 \to 2^+$	$E2$	6.1(8)[71]	0.215(23)	3.1	0.58
	$4^+_3 \to 2^+$	$E2$			0.06	
	$4^- \to 5^-$	$E2$	< 0.3			
	$4^-_2 \to 5^-$	$E2$			0.07	
	$10^+ \to 8^+$	$E2$	31^{+5}_{-4}[70]		2.14	
^{93}Zr	$3/2^+ \to 5/2^+$	$E2$	7(6)	2092(7)	4.45	13870
	$3/2^+_2 \to 5/2^+$	$E2$			0.73	
	$3/2^+_3 \to 5/2^+$	$E2$			0.57	
	$3/2^+_4 \to 5/2^+$	$E2$			1.78	
	$1/2^+ \to 5/2^+$	$E2$			1.61	
	$1/2^+_2 \to 5/2^+$	$E2$			3.71	
	$1/2^+_3 \to 5/2^+$	$E2$			0.002	
	$1/2^+_4 \to 5/2^+$	$E2$			0.67	
	$9/2^+ \to 5/2^+$	$E2$			1.73	
	$9/2^+_2 \to 5/2^+$	$E2$			4.39	
	$9/2^+_3 \to 5/2^+$	$E2$			0.09	
	$9/2^+_4 \to 5/2^+$	$E2$			0.06	
^{94}Zr	$2^+ \to 0^+$	$E2$	4.9(11)[69]	9.9(21)	2.57	19.7
	$2^+_2 \to 0^+$	$E2$	3.9(3)[69]	$3.68^{+0.027}_{-0.023}$	3.27	0.69
	$2^+_3 \to 0^+$	$E2$			1.42	
	$2^+_2 \to 0^+_2$	$E2$	19(2)[69]		1.85	
	$2^+_3 \to 0^+_2$	$E2$	0.04(5)[64]		3.38	
	$2^+_4 \to 0^+_2$	$E2$			0.04	

Continued on next page

Table 2-continued from previous page

^{Z}X	Transition(W.u.)	τL	Exp.	τ/ps	Th.	τ/ps
	$0_2^+ \to 2^+$	$E2$	9.3(4)[69]		1.53	
	$0_3^+ \to 2^+$	$E2$			0.04	
	$0_4^+ \to 2^+$	$E2$			2.23	
	$4^+ \to 2^+$	$E2$	0.88(23)[69]	721(19)	0.55	177
	$4_2^+ \to 2^+$	$E2$	13^{+4}_{-7}[69]	$0.42^{+0.20}_{-0.11}$	4.69	0.85
	$4_3^+ \to 2^+$	$E2$			0.74	
	$4_2^+ \to 2_2^+$	$E2$	34^{+10}_{-7}[69]		3.94	
	$4_3^+ \to 2_2^+$	$E2$			1.67	

both low-lying and high-spin excitations.

The excited states of ^{91}Zr extend to approximately 10 MeV with spin up to $J = 35/2$. By including three monopole correction terms, the energy ordering and positions of low-lying levels (*e.g.*, $5/2^+$, $1/2^+$, $7/2^+$, and $11/2^-$) were significantly improved, bringing them into good agreement with experimental values. The model also satisfactorily reproduces other high-spin states (e.g., $29/2^-$, $33/2^+$, $35/2^+$). Specifically, the $29/2_2^-$ state has a difference factor of 0.96, coupled by orbits $\pi p_{3/2}$, $\pi p_{1/2}$, $\pi g_{9/2}$, and $\nu g_{9/2}$. The $33/2^+$ and $35/2^+$ states have difference factors of 0.96 and 0.98, respectively, coupled by orbits $\pi p_{3/2}$, $\pi p_{1/2}$, $\pi g_{9/2}$, and $h_{11/2}$. The excited levels of ^{92}Zr are properly explained up to approximately 10 MeV with spin $J = 19$. For examples, the low-lying states 2^+, 4^+, and 6^+ properly reproduce the corresponding data with difference factors of 0.97, 1.01, and 0.99, respectively, coupled by orbits $\pi p_{1/2}$, $\pi g_{9/2}$, and $\nu d_{5/2}$. High-spin levels 12_2^+ and 18_2^+ show equal difference factors of 1.04, coupled by orbits $\pi p_{1/2}$, $\pi g_{9/2}$, $\nu d_{5/2}$, and $\nu h_{11/2}$.

The level spectra of ^{93}Zr are properly reproduced well for excited energy exceeding 11 MeV. For example, low-lying levels $1/2^+$, $9/2^+$, and $13/2^+$ have difference factors of 0.98, 1.12, and 1.04, respectively, coupled by orbits $\pi p_{1/2}$, $\pi g_{9/2}$, $\nu d_{5/2}$, and $\nu s_{1/2}$. High levels $43/2^-$, $45/2^-$, and $47/2^-$ have difference factors of 0.99, 0.99, and 1.02, respectively, coupled by orbits $\pi p_{1/2}$, $\pi g_{9/2}$, $\nu d_{5/2}$, and $\nu h_{11/2}$. The level spectra of ^{94}Zr were investigated up to approximately 8 MeV with spin $J = 16$. Low-lying states 2^+, 4^+, and 6^+ have difference factors of 0.92, 1.08, and 0.92, respectively, coupled by orbits $\pi p_{1/2}$, $\pi g_{9/2}$, and $\nu d_{5/2}$. High spin states 14_3^+, 15_2^+, and 16_4^+ have difference factors of 0.96, 1.001, and 0.97, respectively, coupled by orbits $\pi p_{1/2}$, $\pi g_{9/2}$, $\nu d_{5/2}$, $\nu h_{11/2}$, and $\nu d_{3/2}$.

The spectra of $^{91-94}$Zr were investigated under both low-lying and high-spin excitations, and their wave functions were further tested by comparing the electromagnetic transitions probabilities with given $B(E2)$ data. The calculations provide systematic predictions and configuration interpretations for the high-spin states of Zr isotopes. The high performance in both spectra and transitions probabilities makes the predicting calculations of the present interaction more dependable to be referred in further experimental researches of Zr isotopes.

References

[1] M. Quinn, A. Aprahamian, J. Pereira *et al.*, Phys. Rev. C **85**, 035807 (2012)
[2] M. P. Reiter, S. Ayet San Andrés, S. Nikas *et al.*, Phys. Rev. C **101**, 025803 (2020)
[3] R. Yokoyama, R. Grzywacz, B. C. Rasco *et al.*, Phys. Rev. C **100**, 031302 (2019)
[4] C. Fougères, M. L. Avila, H. Jayatissa *et al.*, Phys. Rev. C **109**, 065805 (2024)
[5] S. Han-Feng, Z. Bo, Z. Jiang *et al.*, Chin. Phys. Lett. **20**, 2084 (2003)
[6] A. Banu, E. G. Meekins, J. A. Silano *et al.*, Phys. Rev. C **99**, 025802 (2019)
[7] A. Spyrou, S. J. Quinn, A. Simon *et al.*, Phys. Rev. C **88**, 045802 (2013)
[8] M. Beard, S. Frauendorf, B. Kämpfer *et al.*, Phys. Rev. C **85**, 065808 (2012)
[9] S.-H. Cheng, J. Wen, L.-G. Cao *et al.*, Chin. Phys. C **47**, 024102 (2023)
[10] Y. Zheng, G. d. France, X.-H. Zhou *et al.*, Chin. Phys. C **44**, 024002 (2020)
[11] H. Wang, K.-Y. Ma, Y.-H. Wu *et al.*, Chin. Phys. C **45**, 014001 (2021)
[12] Y.-F. Lv, J.-B. Lu, G.-L. Zhang *et al.*, Chin. Phys. C **43**, 104102 (2019)
[13] B. Sun, F. Montes, L. S. Geng *et al.*, Phys. Rev. C **78**, 025806 (2008)
[14] C. Izzo, J. Bergmann, K. A. Dietrich *et al.*, Phys. Rev. C **103**, 025811 (2021)
[15] P. T. Hosmer, H. Schatz, A. Aprahamian *et al.*, Phys. Rev. Lett. **94**, 112501 (2005)
[16] M. Madurga, R. Surman, I. N. Borzov *et al.*, Phys. Rev. Lett. **109**, 112501 (2012)
[17] P. Hosmer, H. Schatz, A. Aprahamian *et al.*, Phys. Rev. C **82**, 025806 (2010)
[18] G. Tagliente, P. M. Milazzo, K. Fujii *et al.*, Phys. Rev. C **84**, 015801 (2011)

[19] A. Couture, R. F. Casten, R. B. Cakirli, Phys. Rev. C **104**, 054608 (2021)
[20] C. Freiburghaus, S. Rosswog, F.-K. Thielemann, The Astrophysical Journal **525**, L121 (1999)
[21] R. Surman, G. C. McLaughlin, M. Ruffert *et al*., The Astrophysical Journal **679**, L117 (2008)
[22] S.-i. Fujimoto, K. Kotake, S. Yamada *et al*., The Astrophysical Journal **644**, 1040 (2006)
[23] G. Tagliente, K. Fujii, P. M. Milazzo *et al*., Phys. Rev. C **77**, 035802 (2008)
[24] G. Tagliente, P. M. Milazzo, K. Fujii *et al*., Phys. Rev. C **78**, 045804 (2008)
[25] G. Tagliente, P. M. Milazzo, K. Fujii *et al*., Phys. Rev. C **81**, 055801 (2010)
[26] P. Rudling, R. Adamson, in *Materials Ageing and Degradation in Light Water Reactors*, edited by K. Murty (Cambridge: Woodhead Publishing, 2013), p. 246–283
[27] K. Kolos, A. Hennessy, N. Scielzo *et al*., Nucl. Instrum. Methods Phys. Res. A, **1000**, 165240 (2021)
[28] A. Takibaev, M. Saito, V. Artisyuk *et al*., Journal of Nuclear Science and Technology **37**, 870 (2000)
[29] https://www.nndc.bnl.gov/ensdf/
[30] T. Sumikama, K. Yoshinaga, H. Watanabe *et al*., Phys. Rev. Lett. **106**, 202501 (2011)
[31] S. Miyahara, H. Nakada, Phys. Rev. C **98**, 064318 (2018)
[32] P. Banerjee, S. Ganguly, M. K. Pradhan *et al*., Phys. Rev. C **98**, 034320 (2018)
[33] E. V. Mardyban, E. A. Kolganova, T. M. Shneidman *et al*., Phys. Rev. C **105**, 024321 (2022)
[34] W. Witt, V. Werner, N. Pietralla *et al*., Phys. Rev. C **98**, 041302 (2018)
[35] J. E. García-Ramos, K. Heyde, Phys. Rev. C **100**, 044315 (2019)
[36] A. Chakraborty, E. E. Peters, B. P. Crider *et al*., Phys. Rev. Lett. **110**, 022504 (2013)
[37] Z. Ge, M. Reponen, T. Eronen *et al*., Phys. Rev. Lett. **133**, 132503 (2024)
[38] H. B. Lv, G. X. Zhang, B. S. Cai *et al*., Phys. Rev. C **111**, 044311 (2025)
[39] T. R. Routray, P. Bano, M. Anguiano *et al*., Phys. Rev. C **104**, L011302 (2021)
[40] B. Brown, W. Rae, Nucl. Data Sheets **120**, 115 (2014)
[41] H.-K. Wang, Y. Sun, H. Jin *et al*., Phys. Rev. C **88**, 054310 (2013)
[42] C.-F. Jiao, C.-X. Yuan, Nuclear Science and Techniques **36**, 202 (2025)
[43] Z.-X. Wang, G.-X. Zhang, W. Jiang *et al*., Nuclear Science and Techniques **36**, 179 (2025)
[44] O. H. Arroe, J. E. Mack, Phys. Rev. **76**, 873 (1949)
[45] B. A. Brown, P. M. S. Lesser, D. B. Fossan, Phys. Rev. Lett. **34**, 161 (1975)
[46] B. A. Brown, P. M. S. Lesser, D. B. Fossan, Phys. Rev. C **13**, 1900 (1976)
[47] C. M. Baglin, Nuclear Data Sheets **114**, 1293 (2013)
[48] Z. G. Wang, M. L. Liu, Y. H. Zhang *et al*., Phys. Rev. C **89**, 044308 (2014)
[49] C. M. Baglin, Nuclear Data Sheets **113**, 2187 (2012)
[50] A. S. Obeid, O. Burda, M. Chernykh *et al*., Phys. Rev. C **87**, 014337 (2013)
[51] C. Fransen, V. Werner, D. Bandyopadhyay *et al*., Phys. Rev. C **71**, 054304 (2005)
[52] J. K. Dickens, E. Eichler, G. R. Satchler, Phys. Rev. **168**, 1355 (1968)
[53] B. A. Brown, D. B. Fossan, P. M. S. Lesser *et al*., Phys. Rev. C **14**, 602 (1976)
[54] N. Fotiades, J. A. Cizewski, J. A. Becker *et al*., Phys. Rev. C **65**, 044303 (2002)
[55] Y. Hao, Z. Ren, J.-B. Lu *et al*., Phys. Rev. C **111**, 034312 (2025)
[56] J. Knight, D. Hoffman, B. Dropesky *et al*., Journal of Inorganic and Nuclear Chemistry **10**, 183 (1959)
[57] B. L. Cohen, O. V. Chubinsky, Phys. Rev. **131**, 2184 (1963)
[58] I. Talm, Phys. Rev. **126**, 2116 (1962)
[59] B. Arad, J. Boulter, W. Prestwich *et al*., Nuclear Physics A **131**, 137 (1969)
[60] S. X. Guan, C. B. Li, Y. Zheng *et al*., Phys. Rev. C **112**, 014304 (2025)
[61] C. M. Baglin, Nuclear Data Sheets **112**, 1163 (2011)
[62] D. Pantelica, I. G. Stefan, N. Nica *et al*., Phys. Rev. C **72**, 024304 (2005)
[63] D. Abriola, A. Sonzogni, Nuclear Data Sheets **107**, 2423 (2006)
[64] E. Elhami, J. N. Orce, S. Mukhopadhyay *et al*., Phys. Rev. C **75**, 011301 (2007)
[65] E. E. Peters, A. Chakraborty, B. P. Crider *et al*., Phys. Rev. C **88**, 024317 (2013)
[66] S. Hontzeas, D. Marsden, Nuclear Physics A **179**, 193 (1972)
[67] J. B. Ball, R. L. Auble, P. G. Roos, Phys. Rev. C **4**, 196 (1971)
[68] M. Liu, C. Yuan, G. Zhang *et al*., Science China Physics, Mechanics & Astronomy **68**, 122011 (2025)
[69] A. Chakraborty, E. E. Peters, B. P. Crider *et al*., Phys. Rev. Lett. **110**, 022504 (2013)
[70] M. Sugawara, Y. Toh, M. Koizumi *et al*., Phys. Rev. C **96**, 024314 (2017)
[71] C. Fransen, V. Werner, D. Bandyopadhyay *et al*., Phys. Rev. C **71**, 054304 (2005)